

Citation for published version:
Krany, MJ, Bowen, C, Michel, C & Taylor, J 2020, 'Transient Analysis of a Current-Driven Full Wave AC/DC
Converter for Indirect Characterization of Piezoelectric Devices during Energy Harvesting', Energy Technology, vol. 8, no. 3, 1901317. https://doi.org/10.1002/ente.201901317

DOI:

10.1002/ente.201901317

Publication date: 2020

Document Version Peer reviewed version

Link to publication

This is the peer reviewed version of the following article: Krany, M.J., Bowen, C.R., Michel, C. and Taylor, J.T. (2020), Transient Analysis of a CurrentDriven Full Wave AC/DC Converter for Indirect Characterization of Piezoelectric Devices during Energy Harvesting. Energy Technol.., which has been published in final form at https://doi.org/10.1002/ente.201901317. This article may be used for non-commercial purposes in accordance with Wiley Terms and Conditions for Self-Archiving.

University of Bath

Alternative formats

If you require this document in an alternative format, please contact: openaccess@bath.ac.uk

Copyright and moral rights for the publications made accessible in the public portal are retained by the authors and/or other copyright owners and it is a condition of accessing publications that users recognise and abide by the legal requirements associated with these rights.

Take down policyIf you believe that this document breaches copyright please contact us providing details, and we will remove access to the work immediately and investigate your claim.

Download date: 08 Mar 2023

Transient analysis of a current driven full wave AC/DC converter for indirect characterisation of piezoelectric devices during energy harvesting

Marcin J. Kraśny (1), Christopher R. Bowen (1), Coralie Michel (1), John T. Taylor (2)
(1) Department of Mechanical Engineering, (2) Department of Electrical Engineering
University of Bath, Bath, BA2 7AY, UK

Nomenclature:

```
C_p internal capacitance of piezoelectric device; [F]
\omega Angular frequency (\omega = 2\pi/T or \omega = 2\pi f); [rad/s]
f Frequency of the exciting signal; [Hz]
T Time period (1/f); [s]
t Time; [s]
n Cycle number
I_0 Amplitude of generated by piezoelectric device, where I_p = I_0 \sin \omega t; [A]
R_L Load resistance (resistance of the ac-dc converter); [\Omega]
C_L Load capacitance of the ac-dc converter; [F]
A This is a constant 4 \cdot f \cdot C_p \cdot R_L
V_{out} Voltage at the output of the circuit, measured across load resistance (R_L); [V]
Vout(n); V_n Voltage at the output of the circuit at cycle n; [V]
V_{n\,(n\to\infty)} Voltage in the steady state region; [V]
V_0 Voltage derived from the average value of the current in a half cycle of a sinusoid, \frac{2}{\pi}I_0, and the load resistance
q_n Sum of the geometric sequence \sum_{i=0}^{n-1} r^i
r Common ratio of the geometric sequence
```

Abstract

This paper provides a new approach to extract piezoelectric energy harvester properties, namely capacitance and current, from the increase of voltage with time on a storage capacitor after full wave rectification. The work provides a derivation of a more complete expression for the development of the output voltage with time, from which the equilibrium expression employed in earlier publications appears as a limiting case. This new formulation enables an accurate estimate of the sinusoidal driving current and the shunt capacitance to be made without recourse to direct measurement. Using the analysis with both simulated and experimental data, a four-step procedure is proposed that requires only the measurement of the initial slope of the voltage-time profile and the final settling value. This approach allows the much studied method of converting the piezoelectric output into charge stored on a capacitor to provide a unique indirect measurement method of the driving current and device capacitance while the piezoelectric energy harvester operates at a variety of conditions, such as frequency, temperature, stress and strain.

Keywords: current mode, rectifier, harvesting, piezoelectric, intrinsic capacitance

1. Introduction

Energy harvesting using piezoelectric materials provides a means to produce power, typically in the μW to mW range, by conversion of mechanical vibrations or strain into electrical power using inertial or kinematic energy harvesting approaches [1]. Applications for piezoelectric energy harvesting include the provision of autonomous, low-maintenance and self-powered systems, such as wireless sensor networks, structural health monitoring and medical devices and biomedical monitoring with a reduced reliance on batteries or electric cables [2][3][4][5][6][7]. Since the charge created by a piezoelectric device during the application of alternating mechanical load is related to its change in polarisation under tensile or compressive stresses, an alternating current is generated. As a result, methods such as full-wave rectification are used to covert the ac output to dc and the resulting electrical energy is stored on a capacitor. Dell' Anna has provided a detailed overview of the range of power management circuits currently available for piezoelectric energy harvesting [8]. Significant attention has been placed on the optimisation of the load resistance [9],[10] along with improvements using synchronous switching [11] or peak detection [12]. There is also effort on the use of a double stage AC/DC architecture to optimise the DC voltage at the output of the diode bridge rectifier by means of a DC/DC converter equipped with Maximum Power Point Tracking and connected to a battery [13].

In this paper the output of a piezoelectric device when it is driven by a sinusoidal mechanical excitation and terminated in a rectifier-filter-type full wave bridge ac-dc converter is considered. As a result of its simplicity in terms of manufacture and use, it is a highly convenient and much studied method of harvesting the energy output of a piezoelectric device by storing the charge generated on a capacitor. The rectifier is typically a diode bridge and the filter the parallel combination of the load resistance and a capacitor providing a time constant sufficiently large that any residual ripple on the DC output voltage can be ignored. In addition, we consider here the case of low electromechanical coupling (LEC), as defined in [13], although in principle the method can be extended to cases for both weakly and non-weakly electromechanical coupled systems [14]. Following Ottman *et al.* [15] the device is modelled as the parallel combination of a sinusoidal current source and a capacitor (the diodes are treated as ideal devices). The output voltage, and hence the power dissipation in the load, increases with time and it is shown that the resulting profile falls into *two* phases: an initial phase where the voltage increases rapidly followed by a steady state phase when the energy supplied per cycle is in equilibrium with the energy dissipated in the load in the same period.

Previous studies have focussed on optimising the power output of such systems in the steady-state phase of the response. Specifically, Ottman *et al.* [15] assumed that the vibration amplitude is not affected by the load resistance, while Guyomar *et al.* [16] hypothesized that the periodic external excitation and the speed of mass are in phase. More recently, these methods were developed by Shu *et al.* [17], taking into account the global behaviour of the electromechanical system.

In the current paper we present a more detailed analysis of the transient behaviour of the state variables of the circuit at each stage of the rectification and filtering process than has been reported previously. This provides a more complete analytic expression for the output voltage as a function of time than in earlier work and the extra information thus obtained forms the basis of the characterisation method described in section 3.2. This method is presented as a four-step procedure that requires only the measurement of the initial slope of the voltage-time profile and the final settling value of the output voltage. We consider the influence of each of the embedded components on the

rectification process and equations in a simple and understandable form are provided. The proposed method could be of significant benefit for researchers in the process of designing and improving the materials used for energy harvesting and also for electronics engineers responsible for the circuit design of piezoelectric-based, self-powered devices.

The work presented in this paper provides a quick and efficient tool for material characterisation and allows easy performance comparison since it enables accurate estimates of the sinusoidal driving current and the shunt capacitance to be made without recourse to complicated direct measurement and expensive high input impedance electrometers or impedance analysers by simply monitoring the voltage on the storage capacitor with time. What is more important and has not yet been reported in literature to date is that it enables the piezoelectric device to be characterised under the conditions of frequency, temperature, stress and strain experienced by the energy harvester during operation. This is of interest since piezoelectric and dielectric properties of the material, and the device, can change with time, frequency, electric field, temperature and stress.

2. Rectification Model

2.1 Model development

A vibrating piezoelectric element is modelled as a sinusoidal current source I_p in parallel with its internal electrode capacitance C_p . This model was proposed in by Ottman $et\ al$. [15] for the particular case of low electromechanical coupling (LEC) and can be applied also to the analysis of devices such pyroelectric generators [18]. The magnitude of the polarization current I_p varies with the mechanical excitation level of the piezoelectric element. Such a device generates an ac current and is therefore the first stage in an energy harvesting circuit is an ac – dc converter, typically a full-wave rectifier and a smoothing capacitor, C_L , as shown in **Fig. 1**. The driving current is of the form $I_p = I_o$ sin ωt , where $\omega = 2\pi/T$ and T is the period of the vibration source and the dc load is represented by R_L .

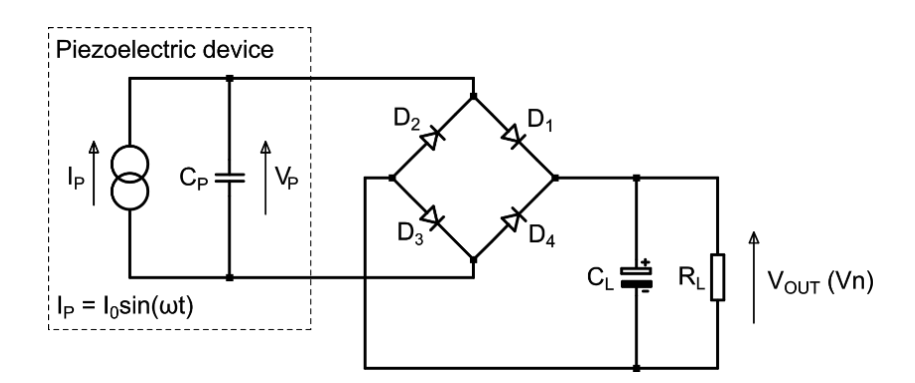


Figure 1. Circuit schematic showing the equivalent circuit of a piezoelectric generator (on the left) connected to a diode bridge ac-dc converter. $I_p = I_o \sin \omega t$.

The operation of this circuit has been described in a variety of references [15]-[17]. However, these references focussed on the steady state behaviour of the voltage output, ignoring the initial transient performance of the state variables. The following analysis begins with the transient behaviour from which the steady state response is derived as a limiting case. For completeness, a brief qualitative

description of the operation of the circuit is given; a more detailed analysis of the full wave bridge rectifier voltage- and current-driven modes are provided in **supplemental materials S1**.

Referring to **Fig 1**, in the first half cycle of operation, assuming a boundary condition that all voltages in the circuit are zero at t = 0, I_P charges the parallel combination of C_P , C_L and R_L , the diodes D_1 and D_3 being forward biased and ON. This phase continues until I_P passes through zero (at the end of the first half cycle, at which point D_1 and D_3 become reverse biased and switch OFF) and subsequently reverses. However, although the driving current now begins to increase negatively and the other pair of bridge diodes D_2 and D_4 are available to conduct in this direction, they cannot do so because the remaining positive voltage on C_P causes them to be reverse biased. D_2 and D_4 remain blocked in this way until the voltage on C_P is discharged by I_P . The effect of this voltage is to make the diodes conduct during part of the duty cycle only, which significantly modifies the circuit behaviour compared to the case where C_P = (i.e. capacitor not connected) and the circuit operation becomes linear. These two phases of operation are described by the two equivalent half circuits shown in **Fig 2**, and **Fig S4**.

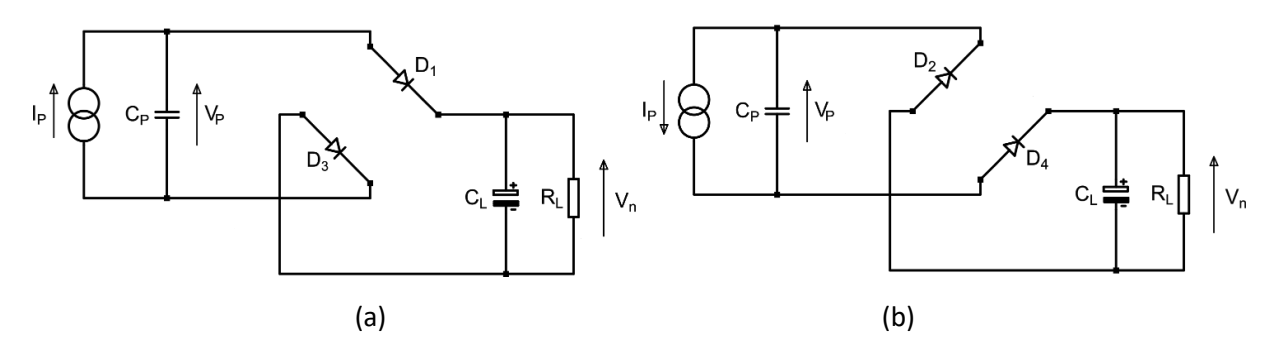


Figure 2. Equivalent half circuits of the circuit of Fig 1. Fig 2(a) describes the operation of the circuit in the half cycles where $I_p = I_o \sin \omega t$ is driving positively and Fig 2(b) for the negative half cycles. Fig 2(b) also indicates the blocking effect of the charge on C_p in the negative half cycles.

The duration of the blocking or *commutation* phase increases progressively as V_{out} increases, reducing the energy transfer from the piezoelectric device to the load, see **Fig 3(a)**. V_{out} rises stepwise monotonically and eventually reaches a limiting (steady state) value, $V_{n (n \to \infty)}$, at which point the energy input is in equilibrium with the energy dissipated in the load, as shown in **Fig 3(b)**. An example of the corresponding current waveform is given in **Fig 4**; these can be compared with in more detailed views of the corresponding current waveforms in **supplement S1**.

In addition to the sinusoidal nature of the driving current, the following model assumptions are made:

- 1. The diodes are ideal and act as ideal switches with no series resistance or dc offset voltage.
- 2. $R_L(C_p + C_L) >> T$ so that the time constant $R_L(C_p + C_L)$ is much longer than the period of the exciting sinusoid, T. This assumption enables the exponential expression for P to be simplified and, crucially, ensures that the sequence describing the development of the output voltage with time, converges. Note that in general we can also state that $C_p << C_L$ since this will be the case in most practical situations. Note however that the value of C_L cannot be increased without limit as this also increases the time to convergence of the process and can render it impractical to use, as discussed in more detail below.

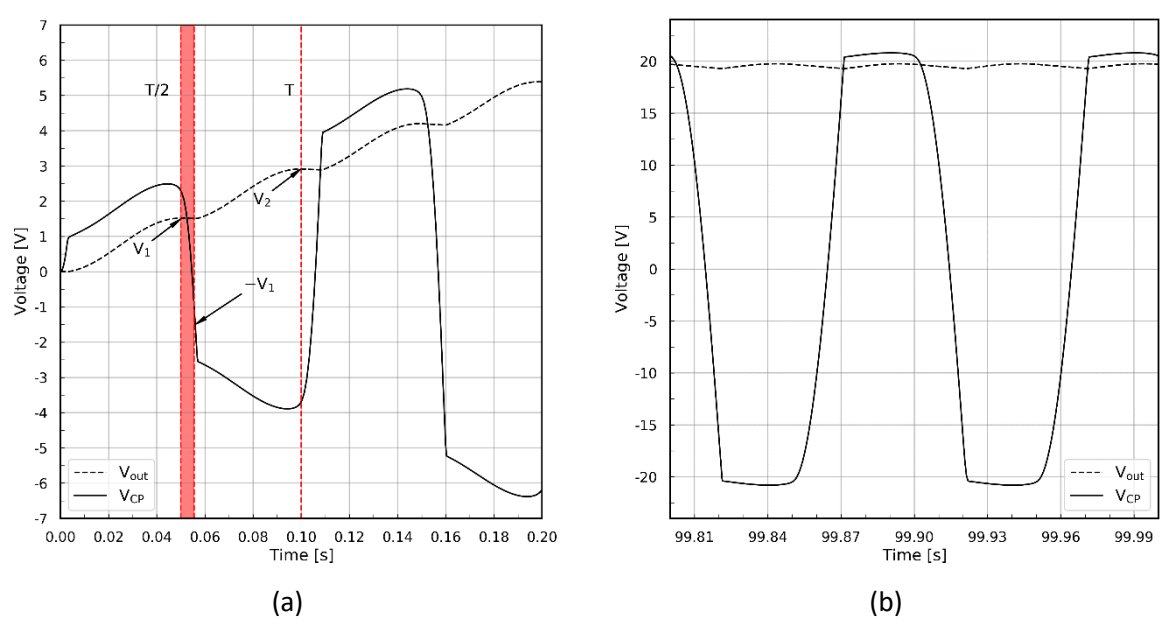


Figure 3. Development of the output voltage (V_{OUT}) with time of the circuit of Fig 1 and the voltage across C_P with time. (a) shows the first few half cycles and the appearance of the blocked phase in the second half cycle, of duration τ_1 (marked with the red vertical block). (b) shows the same pair of voltages at steady state (equilibrium) when V_{OUT} has reached a constant value except for a small residual ripple.

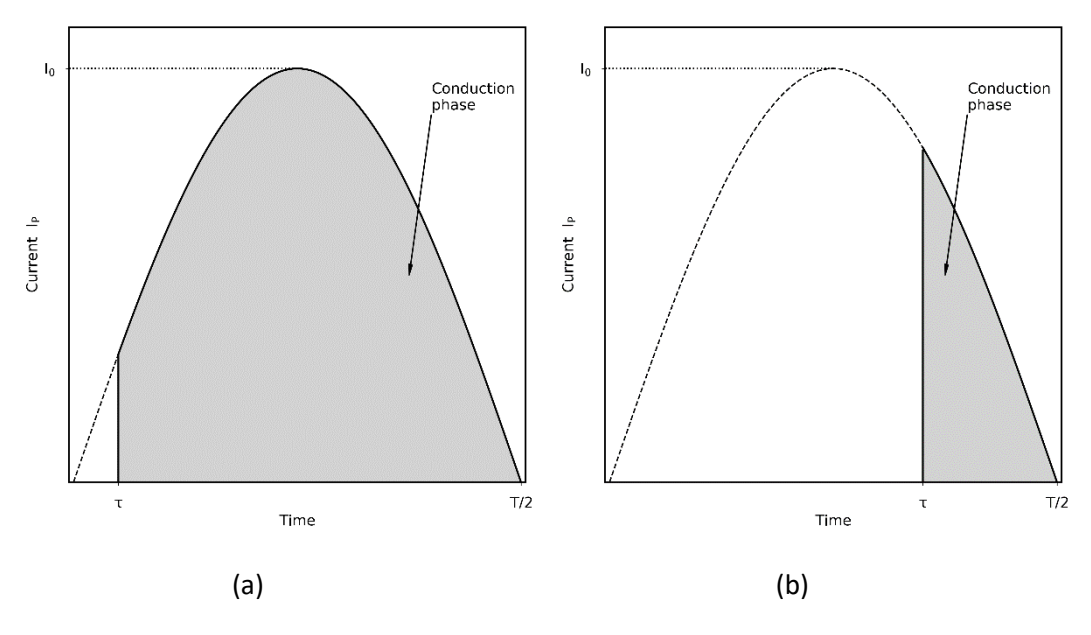


Figure 4. One half cycle of the sinusoidal current I_P , showing the part of the cycle where conduction occurs, i.e. in the range $\tau \le t \le T/2$. (a) shows the conduction phase during first few half cycles (b) shows the same pair of currents at steady state (equilibrium) when V_{OUT} has reached a constant value and experiences short rechargeable pulses to counteract the residual ripple.

2.2. Model analysis

In the first half cycle of operation, termed phase zero: $0 \le t \le T/2$, as already described, C_p , C_L and R_L , are charged by the full positive phase of I_p . For this half cycle the circuit behaves in a linear manner and the first assumption above allows us to calculate V_{out} at $t_1 = T/2$, which we call V_1 :

$$V_1(1) = PV_0 \tag{1}$$

where P is the transient response of an RC circuit [19].

$$P = 1 - e^{-\left(\frac{T}{2}\right)/(C_p + C_L)R_L} \tag{2}$$

and:

$$V_0 = \frac{2}{\pi} I_0 R_L \tag{3}$$

where V_0 is an average voltage derived from the average value of the current in a half cycle of a sinusoid. The term P is a constant depending on physical parameters of piezoelectric device and embedded circuit. Note that using Assumption 2, $R_L(C_p + C_L) >> T$, a simplified expression for P can be derived:

$$P \cong \frac{T}{2(C_p + C_L)R_L} \tag{4}$$

For the next half cycle, i.e. $T/2 \le t \le T$, having passed the peak of the sinusoid, the voltage generated by the piezoelectric declines and current flow through the diodes is blocked by the residual positive voltage, leaving V_1 constant, subject to some leakage through R_L , as indicated in **Fig 3(a)**. This phase lasts until C_P discharges and is subsequently recharged negatively to $-V_1$, so that D_2 and D_4 are turned ON. The time taken for V_P to traverse the region between V_1 and $-V_2$ defines the part of the duty cycle of duration t_1 when the diode bridge is not conducting. This can be seen in the simplified current waveforms in **Fig 4**, and in more detail in **Fig. S5**.

The time taken for this to occur is calculated by analysing the charging behaviour of a capacitor C_p from a sinusoidal source I_p ,

$$I_P(n) = C_P \frac{dV_n}{dt} \tag{5}$$

which after integrating across a half sinusoid from t_n to T/2 can be expressed, for the n^{th} half-cycle, as

$$\cos \omega \tau_n = 1 - \frac{2\omega C_p}{I_o} V_n \tag{6}$$

The average value of the transferred current (I_{av}) in a partially blocked half cycle (see **Fig 4**), where the length of the commutation cycle is $<\tau_n$, T/2> is given by:

$$I_{av} = I_0 \frac{2}{T} \int_{\tau_n}^{T/2} \sin \omega_0 t dt = I_0 \frac{1}{\pi} (1 + \cos \omega_0 \tau_n)$$
 (7)

where as $\tau_n \to 0$, $I_{av} \to 2I_0/\pi$ as expected for the ideal, non-blocking case (see **Eqn 3**). Substituting for $\cos \omega \tau_n$ from **Eqn (6)**, the average value of the current in a partially blocked half sinusoid is:

$$I_{av} = \frac{2I_0}{\pi} \left(1 - \frac{V_n}{V_0} A \right) \tag{8}$$

where the constant A is given by,

$$A = 4fC_pR_L (9)$$

and $f = \omega/2\pi$. This can be normalised to the ideal case where there is no blocking:

$$F = \left(1 - \frac{V_n}{V_0}A\right) \tag{10}$$

The dimensionless, normalised factor *F* given in **Eqn (10)** is a measure of the square root of the energy transmitted to the load normalised to the maximum possible value, i.e. when there is no blocking. In practice, as we have seen, no blocking occurs only in the first half cycle of operation. Using this information, we can now show how the sequence progresses. The output voltage after the next half cycle is therefore:

$$V_2 = V_1 + P(V_0 - V_1) \left(1 - \frac{V_1}{V_0} A \right) \tag{11}$$

Substituting for V_0 from **Eqn (1)**:

$$V_2 = V_1[1 + (1 - P)(1 - AP)] \tag{12}$$

Assumption 2 ensures that $P \ll 1$ and therefore the terms in P^2 and above can be neglected. The expression for V_2 can therefore be rewritten:

$$V_2 = V_1[1+r] \tag{13}$$

where:

$$r = 1 - P(1+A) \tag{14}$$

where *r* is the *common ratio* of the sequence.

Similarly, proceeding as in (Eqn (11)), the expression for the next iteration follows immediately:

$$V_3 = V_1(1+r) + P[V_0 - V_1(1+r)] \left(1 - \frac{V_1(1+r)}{V_0}A\right)$$
 (15)

After rearrangement and neglecting terms in P^2 and above, this can be written:

$$V_3 = V_1(1+r+r^2) \tag{16}$$

Using this approach, it can be shown that the sum of the sequence after *n* iterations is given by the expression:

$$V_n = V_1 \sum_{i=0}^{n-1} r^i = V_1 \cdot q_n \tag{17}$$

Where the sequence q_n is a *geometric progression* and the sum to n terms of such a sequence is given by the expression:

$$q_n = \sum_{i=0}^{n-1} r^i = 1 + r + r^2 + \dots + r^{n-1}$$

$$= \frac{1 - r^n}{1 - r}$$
(18)

And hence eqn (17) becomes:

$$V_n = V_1 \cdot q_n = V_1 \frac{1 - r^n}{1 - r}$$

Where V_1 and r are given by eqns (1) and (14), respectively.

Crucially, an examination of the expression for r (Eqn (14)) shows that applying Assumption 2, $0 \le r \le 1$ and so the sequence q_n converges. As a result, in the limit as $n \to \infty$, Eqn (17) becomes:

$$V_{n(n\to\infty)} = \frac{V_1}{1-r} \tag{19}$$

Substituting for r and V_1 :

$$V_{n(n\to\infty)} = \frac{V_0}{1+A} \tag{20}$$

Eqns (17) and (18) therefore describe the development of the transient output voltage with time, while Eqn (20) is the steady state value of the output voltage and has been reported elsewhere in the literature [15]. It is significant that the final setting value of the output voltage is independent on load capacitance (C_L). Note also that the speed of convergence of the process can be deduced from eqn (18). As $r \to 1$, the time to convergence, namely the point in the sequence when V_n approaches its

final value as determined by **eqns (19)** and **(20)**, tends to infinity. Since from eqn (14) the common ratio r depends on the parameter P and hence the load time constant, the load capacitor C_L cannot be increased without limit, and indicated in section 2.1.

3 RESULTS AND DISCUSSION

3.1 Model validation using circuit simulation

In order to validate the model, a number of examples were simulated in LTspice (Analog Devices) [20] using a standard pn silicon signal diode model (1N4148) and the results compared to **Eqns (17)** and **(20)**. As discussed, a parallel combination of a sinusoidal current source and a capacitor was used to model the piezoelectric energy harvester, see **Fig 1**. The parameters of the simulations are related to fixed values of $C_P = 150$ nF, $C_L = 10$ µF, $R_L = 100$ k Ω , f = 10 Hz and five values of peak driving current I_O : 100 µA, 200 µA, 300 µA, 400 µA, and 500 µA, as shown in **Fig. 1**.

The results of the comparison are given in **Fig 5**. In all cases a high level of agreement between the model equations and the LTspice output is evident in both the initial transient voltage with time and the steady state regions of operation. Note that the model outputs are consistently greater than the LTspice values, since the model does not allow for the ON voltage of the diodes. This is not a problem where the final value of the output is a few volts or more; as in the examples shown in **Fig. 5**. In cases where this voltage is lower, the inclusion of a diode model will be necessary. Finally, it should be noted that the LTspice output voltage contains a small residual ripple voltage due to the finite value of the time constant R_LC_L . Since this does not contribute to the information intended to be gathered by the proposed method, no corresponding model of ripple was included.

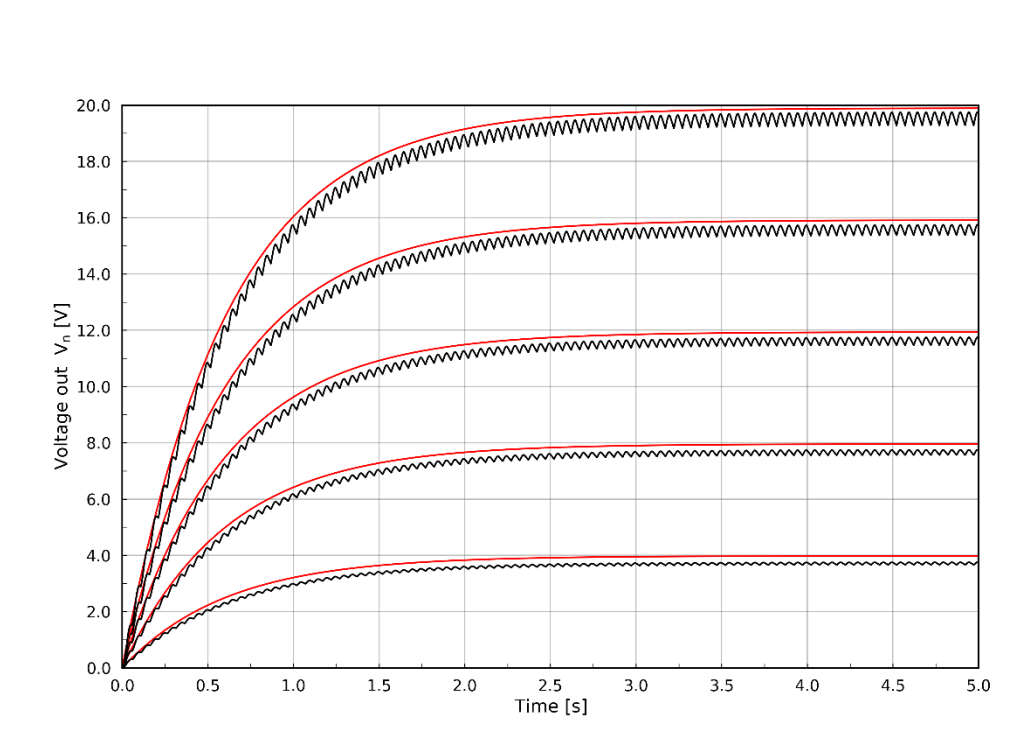


Figure 5. Comparison of model (solid, red traces) with circuit simulation (black traces with ripple) based on parameters given in section 3.1. Beginning at the top the traces shows the results for I_0 = 500 μA, 400 μA, 300 μA, 200 μA and 100 μA. C_P = 150 nF, C_L = 10 μF, R_L = 100 kΩ and f = 10Hz.

3.2 Application of the SPICE model to extract I_0 and C_p from the voltage-time data

The proposed model is successful in calculating the development of the voltage on the storage capacitor C_L with time. We will now show that the model **Eqns (17)** and **(20)** provide a method to estimate directly the two unknown parameters of the working piezoelectric energy harvester, I_0 and C_P using simply the initial slope and final value of the voltage-time profile. This is possible since the development of V_{out} with time falls into two distinct phases, namely the transient (**Eqn (17)**) and steady state (**Eqn (20)**), each with its own characteristic equation shown in **Fig. 6**. Beginning with the sequence in **Eqn (17)**, it can be shown that:

$$r \cong \frac{V_{n(n\to\infty)} - V_1}{V_{n(n\to\infty)}} \tag{21}$$

Furthermore, combining the expression for r (Eqn (14)) with the simplified form of P Eqn (4), the following expression for C_p can be derived:

$$C_P = \frac{2 \cdot R_L \cdot C_L \cdot (1 - r) - T}{2 \cdot R_L \cdot (r - 1) + 4 \cdot R_L}$$
 (22)

Finally, inverting Eqn (20):

$$I_0 = \frac{\pi \cdot V_{n(n \to \infty)} \cdot \left(1 + 4 \cdot f \cdot C_p \cdot R_L\right)}{2 \cdot R_L} \tag{23}$$

where I_0 is the amplitude of the driving sinusoid, I_p .

Using these equations, a four-step parameter extraction procedure can be derived. This is illustrated schematically in **Figure 6**. The procedure is as follows:

- 1. Record the steady state value of the output voltage on $C_L(V_{n(n\to\infty)})$;
- 2. Calculate *r* from the charging curve on the voltage-time profile using **Eqn (21)**;
- 3. Calculate C_p using **Eqn (22)**, r and other known constant parameters (R_L and C_L);
- 4. Calculate I_0 using Eqn (23), $V_{n(n\to\infty)}$, calculated value of C_p (Eqn (22)) and other known parameters (R_L and f).

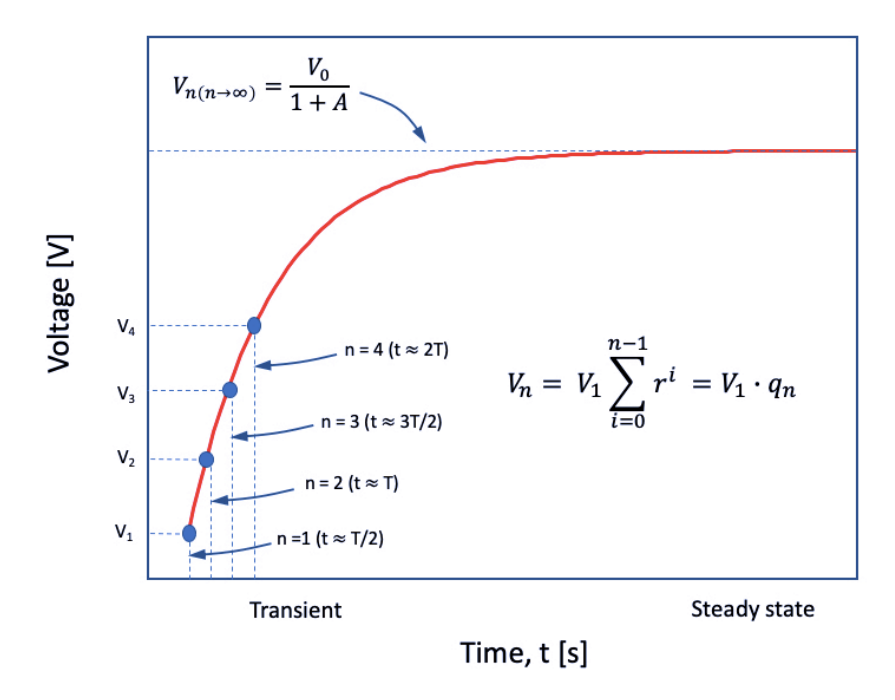


Figure 6. Illustration of the development of the output voltage (voltage on capacitor C_l) with time, showing the transient and steady state regions.

In order to validate the proposed method, **Table 1** and **Fig 7** compare the values for C_p and I_0 obtained using the four-step extraction procedure with the data presented in **Fig 5** that is based on the known values used in the simulations. The resulting values for I_0 and C_p indicate that the proposed procedure provides a good level of accuracy for both these key parameters.

For clarity the data in **Table 1** is repeated in **Fig 7(a)**. It should be noted that the data presented in Table 1 are calculated for the 'RC to T' ratio equal to 10.15, which was chosen as a lowest condition for this parameter in the described case. For 'RC to T' ratio higher than 20 the resulting C_P calculation error is lower than 1.7 % and resulting I_0 error less than 2.0 %. This is because Assumption 2, namely $R_L(C_P + C_L) >> T$, becomes more valid, thereby improving the accuracy of the approximate expression for P, **Eqn (4)**. **Figure 7(b)** is a plot of the extracted values of C_P and I_0 as a function of increasing 'RC to T' ratio from Assumption 2.

Table 1. Extraction of C_P and I_o based on data in **Fig 5** (f = 10 Hz). Percentage error values in parenthesis. Last row in table for I_0 = 1 mA is added to show a limiting case.

<i>I</i> ₀ set [μA]	V ₁ (SPICE)	$V_{n(n \to \infty)}$	r extracted	C _p extracted	I ₀ extracted
	[V]	(SPICE)[V]	(Eqn (21))	[nF] (Eqn (22))	[μΑ] (Eqn (23))
100	0.296	3.754	0.921	149.80 (0.136%)	94.30 (5.70 %)
200	0.601	7.751	0.922	143.49 (4.34 %)	191.62 (4.19 %)
300	0.907	11.752	0.923	141.38 (5.75 %)	288.99 (3.67 %)
400	1.212	15.756	0.923	140.31 (6.46 %)	386.39 (3.40 %)
500	1.518	19.760	0.923	139.66 (6.89 %)	483.79 (3.24 %)
1000	3.048	39.791	0.923	138.34 (7.78 %)	970.90 (2.91 %)

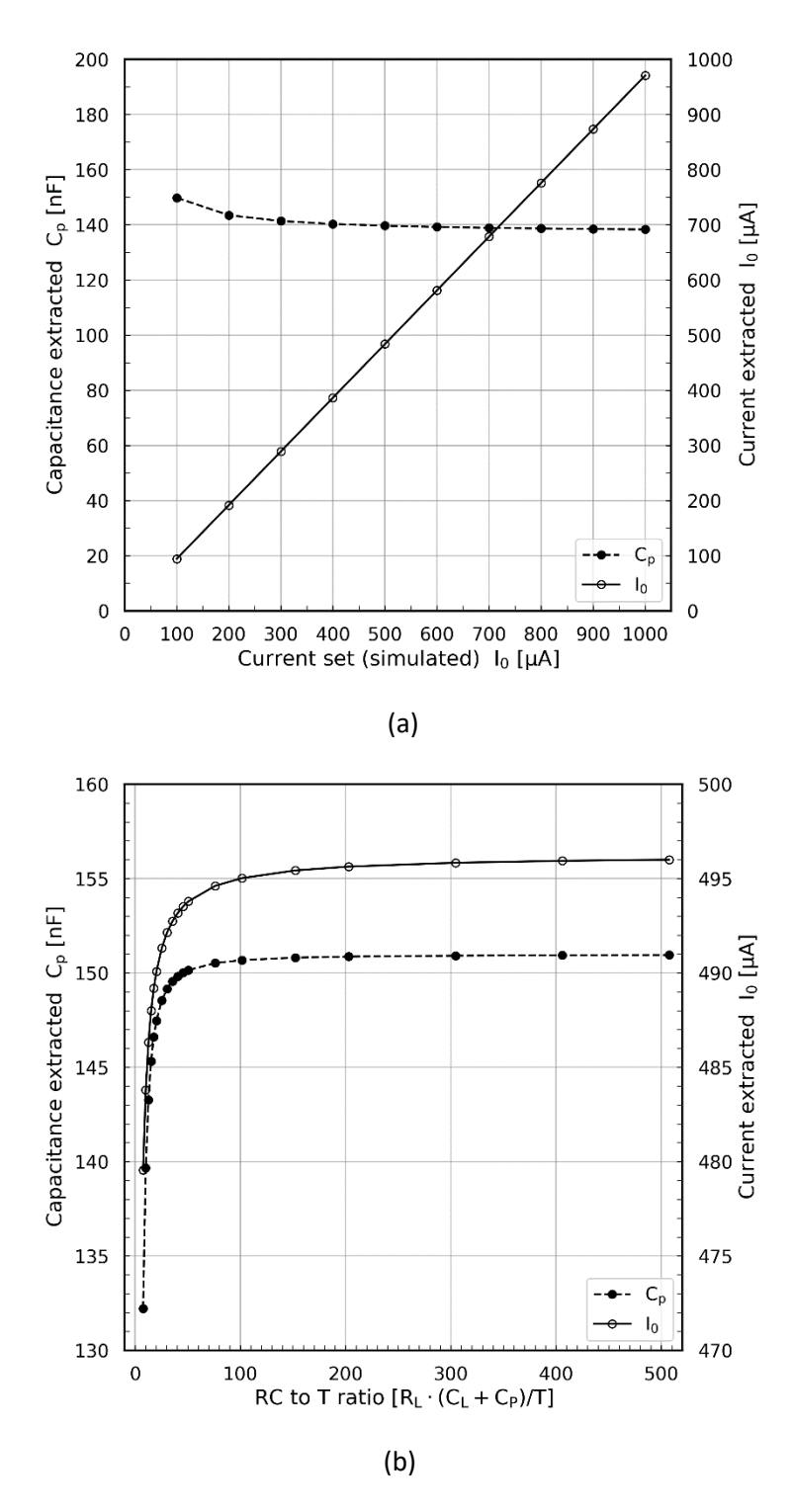


Figure 7. (a) I_0 (solid line) and C_p (dashed line) extracted from (data in **Fig. 5** at 10Hz) vs I_0 simulated in the extended range for up to 1 mA. (b) shows the accuracy of the extracted values of I_0 (solid line) and C_p (dashed line) with increasing RC to T ratio from the *Assumption 2*. The nominal values are $I_0 = 500 \, \mu\text{A}$, $C_p = 150 \, \text{nF}$, $C_L = 10 \, \mu\text{F}$, R_L from 100 kΩ to 5 MΩ.

3.3 Application of method to real experimental data.

We now apply the approach described in the previous sections to a real piezoelectric energy harvesting configuration and extract I_0 and C_p from experimental data. A commercially available Macro Fibre Composite (MFC) patch (MFC2414-P2) [21] with an active area of 24mm by 14mm was mounted on a carbon reinforced fibre matrix (CRFM) cantilever beam of dimensions (300 mm length, 60 mm wide and 0.5 mm thick) using epoxy resin (ARALDITE Standard). The manufacturing process of the beam is described in detail by Harris et al. [22]. The beam was clamped in a holder constructed from two metal plates (29 mm wide, 88 mm length and 2.6 mm thick) and mounted on an electrodynamic shaker (LDS V455) in the same manner as described by Harris [22]. The shaker was driven by the signal generated by a Keysight 33210A function generator amplified by the LDS PA1000 amplifier. Initially the voltage output from the beam was scanned in the frequency sweep mode from 5-50 Hz at a constant acceleration of 0.5 g (4.9 m/s²) to find the mechanical resonance frequency, at which the energy produced by the MFC patch is maximum. The first resonance mode was found at 6.5 Hz, followed by a second mode at 35 Hz. As the first resonance frequency results in the highest output signal, experiments were carried out using this mode. The combination of a relatively large area piezoelectric element and mechanical oscillation at the resonance frequency of the structure leads to a relatively large piezoelectric charge with short circuit currents in excess of 100 μA and open circuit voltages in excess of 40V; this experimental configuration was selected to minimise any errors due the resulting voltage drop introduced by the diodes in the rectifying circuit. The unclamped capacitance (constant stress capacitance) of MFC2414-P2 patch was measured with an impedance-phase analyser (Solartron 1260) with a dielectric interface (Solartron 1296) with 0.1 V_{RMS} signal at 6.5 Hz and was 32.0 nF. Capacitance measured with a standard LCR meter (HP 4263B with 1 V_{RMS} signal at 100 Hz) was 31.3 nF. The claimed functionality of a piezoelectric generator modelled and simulated as a constant current source was proven with various load resistances and is described in detail in supplement S2.

The piezoelectric harvester was connected to a full wave bridge rectifier constructed from four 1N4148 (NXP Semiconductors) diodes with C_L = 10 μ F (Rubycon radial aluminium electrolytic LLE series, 200V capacitance measured with LCR meter at 100 Hz was 9.99 μ F) and R_L = 500 k Ω (PeakTech 3265 resistance decade) as in the circuit schematic presented in **Fig. 4**. Since the piezoelectric charge Q generated is proportional to stress (and strain) and therefore the amplitude of the piezoelectric current (I_0) should be proportional to the excitation level the cantilever was driven with increasingly large accelerations of amplitude 0.2g, 0.5g, 0.8g and 1g, which correspond to short circuit currents I_0 of 30 μ A, 66 μ A, 103 μ A and 124 μ A (**Table 2**); further detail is shown in **supplement S3**. The voltage on C_L capacitor was measured as a function of time with an electrometer's (Keithley 6517B) analogue output connected to oscilloscope (Agilent DSO-X 2024A), responsible for recording of the charging curve. Initially the C_L capacitance and intrinsic piezoelectric capacitance C_P were discharged and then short-circuited to ensure no residual charge was stored in those capacitances. Then full charging cycle, for given excitation was repeated 3 to 5 times.

From the recorded signal, the values of C_p and I_0 were calculated and results are presented in **Table 2** and **Fig 8**.

Table 2. Extraction of C_P and I_o based on experimental data in **Fig 9**. Measurement error values in parenthesis are standard deviations.

Excitation acceleration	Measured I ₀ [μA]	Calculated C_p [nF]	Calculated I ₀ [μA]
[g]		(Eqn (22))	(Eqn (23))
0.2	30.32 (+/- 0.53)	42.5 (+/- 3.8)	29.47 (+/- 0.58)
0.5	66.12 (+/- 1.09)	43.6 (+/- 2.9)	61.32 (+/- 1.67)
0.8	102.70 (+/- 1.63)	46.1 (+/- 2.0)	92.68 (+/- 1.30)
1.0	124.39 +/- 2.30	43.1 (+/- 2.0)	106.49 (+/- 1.20)

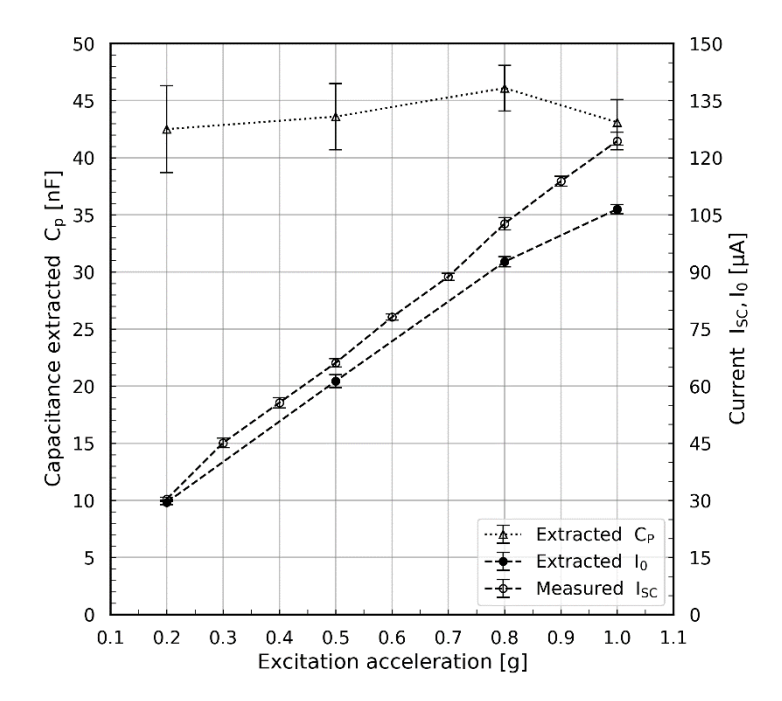


Figure 8. Comparison with measured I_0 and calculated short circuit current and capacitance. Error bars represent standard deviations.

The capacitance (C_P) extracted from the experimental data using the 4-step procedure described above with the use of equation (22) is a stable value, relatively independent of the level of excitation (average $C_P \approx 44.2$ nF) applied to the piezoelectric device.

The amplitude of the current I_o was similarly calculated and compared to the short circuit current produced by the device. Calculated current values (using **Eqn (23)**) increase with amplitude of excitation due to the increase in strain and therefore charge generation, as expected and are within 10 % of the values obtained by direct measurement. The accuracy of I_P current extraction could be increased by calculating the P value with the previously extracted C_P (**Eqn (22)**) value using **Eqn (2)** and substituting this value into the inverted **Eqn (3)** to solve for I_P .

Figure 9 is a plot of the measured output voltage as a function of time for the four values of acceleration used in the experiment, compared to the output of the proposed model calculated for the extracted values of I_0 and averaged value of C_P (44.2 nF).

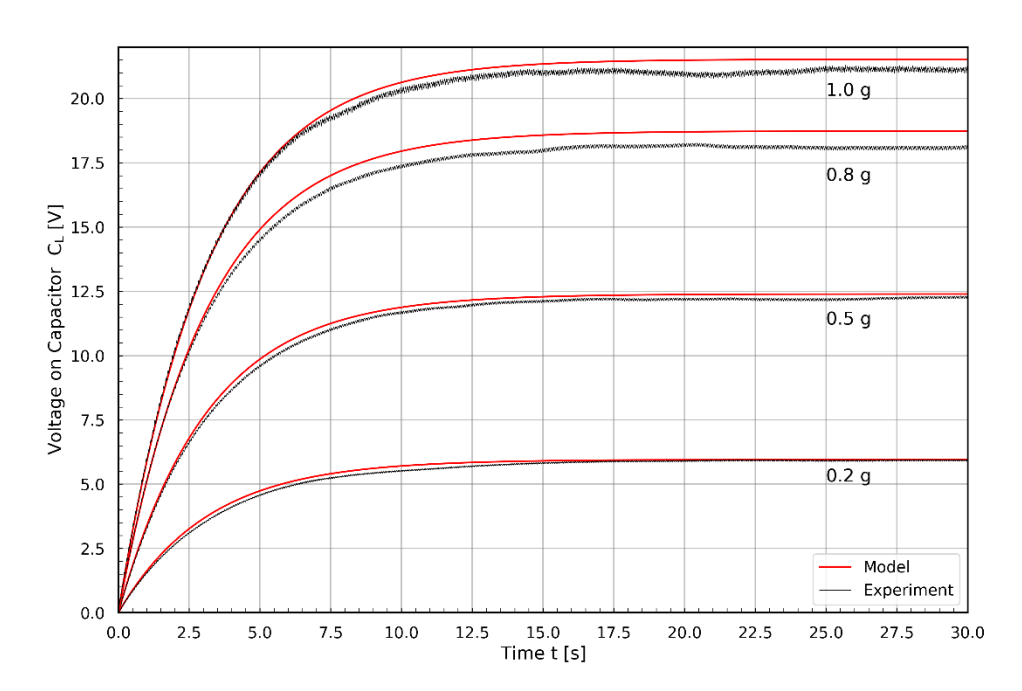


Figure 9. Comparison of model (solid, red traces) with experimental data (black traces with ripple) based on parameters presented in **Table 2**. Beginning at the top the red traces shows the results for I_0 = 106.49 μ A, 92.68 μ A, 61.32 μ A and 29.47 μ A. C_p = 44.2 nF, C_L = 10 μ F, R_L = 500 $k\Omega$ and f = 6.5 Hz.

The above case was also simulated with LTspice with the initial values of C_P = 32.0 nF and (measured short circuit currents) I_0 of 30.32 μ A, 66.12 μ A, 102.70 μ A and 124.39 μ A. The averaged value of retrieved C_P was 31.5 nF and retrieved values of I_0 are calculated with error smaller than 2 %. Further detailed analysis is shown in **supplement S6**. Note that given the values of C_L , R_L and the extracted value of C_P , the 'RC to T' ratio from *Assumption 2* is 32.6.

However, the value of C_p extracted from experimental data is larger (44.2 nF) than the measured capacitance under zero excitation (32.0 nF). The greater values of capacitance calculated using **Eqn** (23) in comparison with the low signal measurement performed with an LCR meter are thought to be a result of electromechanical damping [23]-[26]. The origin of losses of energy harvesting system is in dielectric, piezoelectric, electrical and mechanical change of device's parameters under the influence of operating conditions. This can include dielectric dissipation, permittivity, friction, a stiffness change of the cantilever and piezo-ceramic, electrical losses transformed into heat or wasted during energy conversion. Due to the complex and nonlinear behaviour of these parameters an estimation of all of the above damping sources is a complex task. Damping effects of the system could be replaced by an equivalent C_X capacitance placed in parallel to the C_P intrinsic capacitance, where value of the introduced capacitance is the difference between experimentally measured value and low signal piezoelectric capacitance; in this case $C_X = 12.2$ nF. The introduced additional capacitance (C_X) would represent the damping ratios due to the electromechanical losses experienced by an active piezo-device during energy-harvesting.

In summary we present simple yet effective method to estimate electromechanical losses of the operated energy harvester in a simple equivalent form of an additional capacitance, easily calculated from the simple experiment with a basic circuit based on full wave bridge rectifier. Interestingly the majority of piezoelectric characterisation is undertaken using direct methods, such as an LCR meter or impedance analyser is only possible with the piezoelectric element at steady (not stressed) conditions and at low electric field. However, the indirect approach presented here provides opportunities to characterise the properties of a piezoelectric energy harvesting device at the operating of conditions at high excitation levels, and high stress/strain levels without need to complex characterisation methods; this can be particularly attractive at excitation levels where there is potential for non-linear behaviour in mechanical and/or electrical properties of the harvester [26]. The approach is also valid for sinusoidal thermal fluctuations such as those applied during pyroelectric coefficient characterisation or pyroelectric thermal harvesting where similar rectification methods are employed [11] [18].

6. Conclusions

The present work provides the derivation of a new, complete expression for the development of the output voltage with time of a vibrating piezoelectric energy harvester for the case of low electromechanical coupling (LEC), from which the equilibrium expression employed in several earlier publications appears as a limiting case. This more complete formulation of the problem enables accurate estimates of the sinusoidal driving current (effectively the short circuit current of the harvesting) and the shunt capacitance (effectively the device capacitance) to be made without recourse to direct measurement.

This provides a novel approach to measure indirectly the driving current (which is related to the piezoelectric coefficient of the piezoelectric) and device capacitance (which is related to material permittivity) under the conditions of frequency, temperature, stress and strain experienced by the piezoelectric energy harvester during operation. This enables a more detailed understanding of the behaviour of a piezoelectric energy harvesting device under its driving conditions without need to complex characterisation tools or methods. This is of interest since the piezoelectric and dielectric properties of the harvesting device can change while the harvester is operating at a range of conditions; which include time, frequency, electric field, temperature and stress. There is potential to include a diode model and resulting voltage drop to improve the accuracy of predicted *Cp* and *Ip* values and apply it to more sophisticated rectifying circuits, such as switching inductors.

Acknowledgement

Bowen acknowledges ERC project (ERC-2017- PoC-ERC-Proof of Concept, grant no. 789863)

References

- [1] C. R. Bowen, H. A. Kim, P. M. Weaver, and S. Dunn, 'Piezoelectric and ferroelectric materials and structures for energy harvesting applications', *Energy Environ. Sci.*, vol. 7, no. 1, pp. 25–44, Dec. 2013.
- [2] Z. L. Wang, J. Song, Piezoelectric nanogenerators based on zinc oxide nanowire arrays, *Science*, 312, 242-246, 2006
- [3] X. Wang, J. Song, J. Liu, Z. L. Wang, Direct-current nanogenerator driven by ultrasonic waves, *Science*, 2007, 316, 102-105, 2007.
- [4] R. Yu, C. Pan, J. Chen, G. Zhu, Z.L.Wang, Enhanced performance of a ZnO nanowire-based self-powered glucose sensor by piezotronic effect, *Adv. Funct. Mater.*, 23, 5868-5874, 2013
- [5] Q. Yang, Y. Liu, C. Pan, J. Chen, X. Wen, Z. L. Wang, Largely enhanced efficiency in ZnO nanowire/p-polymer hybridized inorganic/organic ultraviolet light-emitting diode by piezophototronic effect, *Nano Lett.*, 13, 607-613, 2013
- [6] C. Yan, W. Deng, L. Jin, T. Yang, Z. Wang, X. Chu, H. Su, J. Chen, W. Yang, Epidermis-inspired ultrathin 3D cellular sensor array for self-powered biomedical monitoring, *ACS Appl. Mater. Interfaces*, 10, 41070, 2018.
- [7] H. Liu, J. Zhong, C. Lee, S.-W. Lee, and L. Lin, 'A comprehensive review on piezoelectric energy harvesting technology: Materials, mechanisms, and applications', *Appl. Phys. Rev.*, vol. 5, no. 4, p. 041306, Dec. 2018.
- [8] F. G. Dell'Anna *et al.*, 'State-of-the-Art Power Management Circuits for Piezoelectric Energy Harvesters', *IEEE Circuits Syst. Mag.*, vol. 18, no. 3, pp. 27–48, thirdquarter 2018.
- [9] J. T. Scruggs, 'On the Causal Power Generation Limit for a Vibratory Energy Harvester in Broadband Stochastic Response', *J. Intell. Mater. Syst. Struct.*, vol. 21, no. 13, pp. 1249–1262, Sep. 2010.
- [10] F. Lu, H. P. Lee, and S. P. Lim, 'Modeling and analysis of micro piezoelectric power generators for micro-electromechanical-systems applications', *Smart Mater. Struct.*, vol. 13, no. 1, p. 57, 2003.
- [11] K. Makihara, Y. Yamamoto, K. Yoshimizu, C. Horiguchi, H. Sakaguchi, and K. Fujimoto, 'A novel controller to increase harvested energy from negating vibration-suppression effect', *Smart Mater. Struct.*, vol. 24, no. 3, p. 037005, Mar. 2015.
- [12] L. Karthikeyan and B. Amrutur, 'Signal-powered low-drop-diode equivalent circuit for full-wave bridge rectifier', *IEEE Trans. Power Electron.*, vol. 27, no. 10, pp. 4192–4201, 2012.
- [13] M.Balato, L. Costanzo, A. L. Sciavo, M. Vitelli, Optimization of both perturb & observe and open circuit voltage MPPT techniques for resonant piezoelectric vibration harvesters feeding bridge rectifiers, *Sensors and Actuators A*, 278, 85-97, 2018.
- [14] L. Costanzo, A. Lo Schiavo and M. Vitelli, "Power Extracted From Piezoelectric Harvesters Driven by Non-Sinusoidal Vibrations," IEEE Transactions on Circuits and Systems I: Regular Papers, vol. 66, no. 3, pp. 1291-1303, 2019.
- [15] G. K. Ottman, H. F. Hofmann, A. C. Bhatt, and G. A. Lesieutre, 'Adaptive piezoelectric energy harvesting circuit for wireless remote power supply', *IEEE Trans. Power Electron.*, vol. 17, no. 5, pp. 669–676, Sep. 2002.
- [16] D. Guyomar, A. Badel, E. Lefeuvre, and C. Richard, 'Toward energy harvesting using active materials and conversion improvement by nonlinear processing', *IEEE Trans. Ultrason. Ferroelectr. Freq. Control*, vol. 52, no. 4, pp. 584–595, 2005.
- [17] Y. C. Shu and I. C. Lien, 'Analysis of power output for piezoelectric energy harvesting systems', Smart Mater. Struct., vol. 15, no. 6, p. 1499, 2006.
- [18] C. R. Bowen, J. Taylor, E. LeBoulbar, D. Zabek, A. Chauhan, and R. Vaish, 'Pyroelectric materials and devices for energy harvesting applications', *Energy Environ. Sci.*, vol. 7, no. 12, pp. 3836–3856, Nov. 2014.
- [19] John D. Ryder, Electronic fundamentals and applications, 3rd ed. London: Pitman, 1964.

- [20] E. Mike, LTspice. Analog Devices, 2019.
- [21] 'MFC'. [Online]. Available: https://www.smart-material.com/MFC-product-main.html. [Accessed: 05-Sep-2019].
- [22] P. B. Harris, C. R. Bowen, D. N. Betts, and A. H. Kim, 'Manufacture and characterisation of piezoelectric broadband energy harvesters based on asymmetric bistable laminates', 2014.
- [23] A. M. González, Á. García, C. Benavente-Peces, and L. Pardo, 'Revisiting the Characterization of the Losses in Piezoelectric Materials from Impedance Spectroscopy at Resonance', *Materials*, vol. 9, no. 2, p. 72, Jan. 2016.
- [24] M. Goldfarb and L. D. Jones, 'On the efficiency of electric power generation with piezoelectric ceramic', *J. Dyn. Syst. Meas. Control*, vol. 121, no. 3, pp. 566–571, 1999.
- [25] D. A. Hall and P. J. Stevenson, 'High field dielectric behaviour of ferroelectric ceramics', *Ferroelectrics*, vol. 228, no. 1, pp. 139–158, 1999.
- [26] D. A. Hall, 'Review Nonlinearity in piezoelectric ceramics', *J. Mater. Sci.*, vol. 36, no. 19, pp. 4575–4601, Oct. 2001.